Defence Science Journal, Vol. 74, No. 6, November 2024, pp. 787-794, DOI : 10.14429/dsj.74.19382


# Numerical Evaluation on Performance Analysis of Settling Chamber in Tri-Sonic Wind Tunnel

K. Balaji[#], H. Sathish[#], G. Balu[$], V. Shanmugam[$], Prakash Singh[$], V. Gautham[#], C. Vasantharaj[#] and P.S. Prem Kumar[!,*]

[#]*Kumaraguru Centre for Industrial Research and Innovation, Kumaraguru College of Technology, Coimbatore - 641 049, India*
[$]*DRDO-Directorate of Aerodynamics, Defence Research & Development Laboratory, Hyderabad - 500 058, India*
[!]*Department of Aeronautical Engineering, Kumaraguru College of Technology, Coimbatore - 641 049, India*
[*]*E-mail:premkumar.ps.aeu@kct.ac.in*

**ABSTRACT**

The Tri-Sonic wind tunnel under consideration for this study will include a 425 mm×425 mm test section and will produce three speeds: subsonic, transonic, and supersonic. The test will last 30-40 sec and will have a Mach number range of 0.4 to 4.0. This tunnel functions based on the intermittent blow-down concept, wherein a reservoir of high-pressure air, kept at 20 bar, is subsequently released through a nozzle to attain the desired test Mach number. The steady flow inside the test section is hindered by both choking effects and turbulent air downstream of the Pressure Regulatory Valve (PRV), causing the settlement of the boundary layer. Furthermore, it can contribute to significant levels of uncertainty in observed data on the model, thus these pressure fluctuations and turbulent flows must be reduced before they enter the test section. To address this, a series of numerical simulations were conducted under three distinct mass-flow rate conditions, utilizing the turbulence model of k-ω Shear Stress Transport (SST). It was found that the flow recirculation or separation occurred before and after the flow through the Perforated Plate-1. After passing through the second perforated plate, flow recirculation is fully eliminated. This results in less flow recirculation and loss reduction due to flow separation. As a result, it is possible to deduce that the perforated plates greatly help to decrease pressure loss after settling. A honeycomb is put in a constant area section of the settling chamber after the perforated plates. Due to honeycombs' greater ability to diminish lateral turbulence compared to axial turbulence, the flow achieves a higher degree of uniformity following its passage through them. The honeycomb is followed by a wire mesh, which reduces axial turbulence more than lateral turbulence. Ultimately, the settling chamber located downstream of the honeycomb assembly experiences a consistent flow characterised by an average turbulence intensity level of under 1 %.

**Keywords:** Tri-Sonic wind tunnel; Settling chamber; Perforated plate; Pressure regulating valve

## NOMENCLATURE

| | |
|---|---|
| $\Delta P$ | : Pressure loss |
| $A_{flow}$ | : Effective flow cross-sectional area |
| $A_{total}$ | : Cumulative cross-sectional area |
| $D_h$ | : Honeycomb cell diameter |
| DRDL | : Defence Research and Development Laboratory |
| $F_u$ | : Turbulence reduction factor |
| K | : Pressure loss coefficient |
| L/W | : Side ratio |
| $L_h$ | : Internal honeycomb cell length |
| $\dot{m}$ | : Mass flow |
| PP | : Perforated plate |
| PRV | : Pressure regulatory valve |
| $P_s$ | : Static pressure |
| Re | : Reynolds number |
| SST | : Shear stress transport |
| V | : Velocity of the fluid |
| $\beta$ | : Porosity |
| $\rho$ | : Density of air |

Received : 16 August 2023, Revised : 22 April 2024
Accepted : 25 April 2024, Online published : 25 November 2024

## 1. INTRODUCTION

The Tri-Sonic Wind tunnel can produce three-speed regimes in the test section, namely Subsonic, Transonic, and Supersonic. DRDL is currently in the process of constructing a Tri-Sonic wind tunnel featuring a test section measuring 425 mm x 425 mm, designed for the testing of aerospace vehicles. The envisioned test duration spans from 30 to 40 seconds, covering a Mach number spectrum of 0.4 to 4.[1-2] This tunnel configuration will be characterized as an intermittent blow-down system, where high-pressure air, stored at 20 bar, is expanded through a nozzle to attain the necessary Mach number for testing purposes. The depicted wind tunnel in Fig. 1 is composed of several components, including a storage tank, a Pressure Regulating Valve (PRV), a settling chamber, a nozzle, a test section, and a variable-area supersonic diffuser. The air downstream of the PRV will be clogged and highly turbulent. The non-uniformity and

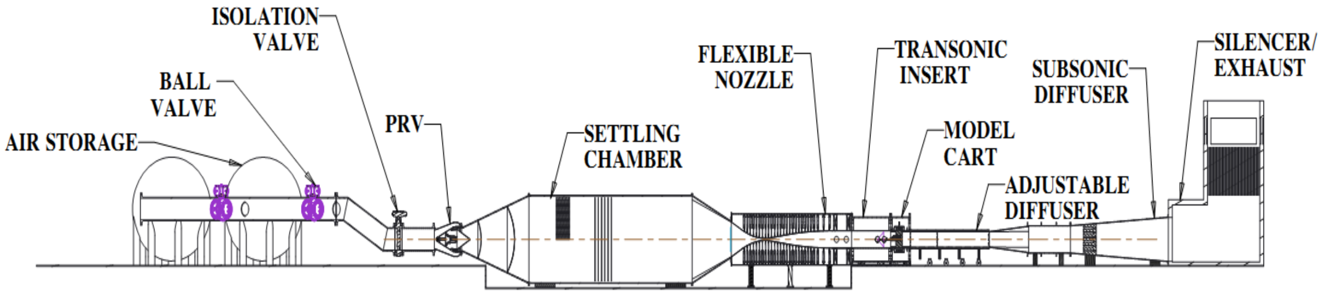


**Figure 1. Schematic diagram of tri-sonic wind tunnel.**

unsteadiness of the flow in the test section will have an adverse effect on the quality of the measured data and may result in the transition of boundary layer position[3-5]. It can also contribute to substantial uncertainty in the model's measured data. To effectively mitigate these pressure fluctuations and attenuate flow turbulence prior to its introduction into the testing section, the implementation of a settling chamber preceding the nozzle becomes imperative. This strategic incorporation of a settling chamber acts as a transformative intermediary, converting the initial high-turbulence flow into a state characterized by diminished turbulence and sustained low-pressure oscillations, as substantiated by scholarly source[6-8]. Notably, the cross-sectional dimension of the expansive-angle diffuser undergoes a swift augmentation, facilitating the attainment of the mandated area ratio across a concise spatial extent. This is bound to cause separation, which can be avoided by adding perforated plates at well-chosen locations. The straight cylindrical portion has a honeycomb flow modifier followed by turbulence-reducing wire mesh screens. This is followed by a converging section. A honeycomb and wire mesh screen combination is used in the straight section to reduce turbulence[9-10]. Based on the contraction ratio, the contraction cone will be designed to make a smooth transition from an upstream circular cross-section to a rectangular cross-section with a 425 mm width and 295 mm height at the exit. Table 1 depicts the critical operating conditions of the tri-sonic wind tunnel.

**Table 1. Critical operating conditions of the tri-sonic wind tunnel**

| Case | 1 | 2 | 3 |
|---|---|---|---|
| Total pressure $P_0$ (bar) | 2.5 | 8.5 | 23 |
| Inlet static pressure $P_s$(bar) | 3.35 | 8.98 | 22.6 |
| Target mass flow rate(kg/s) | 75 | 300 | 87 |
| Turbulence intensity (%) | 20 | 20 | 20 |

## 2. MODELING APPROACH

### 2.1 Modeling of Perforated Plates

In the absence of flow manipulation mechanisms, the effluent from the diffuser assumes the form of an axial jet enveloped by a substantial zone of counter-directed flow. A sector characterised by elevated axial velocity takes shape within the diffuser's central axis zone and endures along its trajectory.

The airflow undergoes acceleration as it moves across the perforated panels, emerging from the openings as a combination of jet streams and swirling currents due to the solid profile of the plate causing obstruction. As the airflow continues downstream, the merging of these jets and swirling currents results in a more even flow.

The degree of irregularities in the flow pattern becomes particularly pronounced when using perforated panels with lower porosity[11]. This effect mandates a greater axial span for the merging of the jets and ambient fluid, prompting the advisability of circumventing the utilization of perforated panels at the diffuser's outlet.

In accordance with Sachin, B.[12-13], *et al.* findings optimal homogeneity in downstream velocity distributions post-diffuser is attained by the deployment of twin perforated panels featuring a porosity (β) value of 0.5.

The optimal outcomes are observed when a single panel is placed right after the entry plane of the diffuser (at L/W=0.14), and the second panel is positioned just before the exit plane (at L/W=0.79). Owing to the concave nature of the perforated plates, the flow through the apertures remains parallel to the surface of the expansive-angle diffuser, thereby curtailing the occurrence of flow separation.

### 2.2 Modeling of Honeycomb

Utilising a honeycomb structure configured with cells oriented parallel to the dominant flow direction offers a valuable strategy for mitigating transverse velocity fluctuations. This advantage stems from the honeycomb's remarkable attribute of inducing minimal pressure drop across its structure, resulting in negligible alterations to the velocity aligned with the primary stream direction. The honeycomb, therefore, emerges as an exceptionally efficient mechanism for rectifying and aligning flow patterns.

However, its efficacy is constrained when addressing fluctuations or non-uniformities that are within the primary stream-wise component. Despite this limitation, the honeycomb proves highly effective in curtailing variations along the orthogonal cross-stream direction. A significant feature of honeycomb design pertains to its dimensions, specifically the diameter of individual cells ($D_h$) and the porosity (β) of the structure.

Honeycomb porosity is defined as the usable cross-sectional area through which fluid can pass to the overall cross-sectional area that encompasses the entire honeycomb structure. This ratio is mathematically represented as:

$$\beta_h = \frac{A_{flow}}{A_{total}} \tag{1}$$

In the realm of wind tunnel honeycomb design, adherence to two principal criteria holds paramount importance. The initial criterion dictates that the proportion of the honeycomb's length ($L_h$) to the diameter of its individual cells ($D_h$) must fall within the range of 6 to 8:

$$6 \leq \frac{L_h}{D_h} \leq 8 \tag{2}$$

The second crucial criterion mandates that the calculated honeycomb porosity ($\beta_h$) should be equal to or greater than 0.8:

$$\beta_h \geq 0.8 \tag{3}$$

For optimal effectiveness, the honeycomb is recommended to possess a thickness of 6 to 8 times the diameter of its cells, ensuring the presence of approximately 150 cells per diameter of the settling chamber. This configuration maximizes the advantageous attributes of the honeycomb structure.

Detailed specifications of the honeycomb parameters employed in the context of this study are accurately outlined in Table 2, providing a comprehensive reference for their utilisation and impact.

**Table 2. Honeycomb parameters**

| Parameters | |
|---|---|
| Cell Size | 25.4 mm |
| Cell length | 210 mm |
| Cell thickness | 2.4 mm |
| Porosity ($\beta_h$) | 0.93 |
| Cell length / size | 8 |

### 2.3 Modeling of Screens

Screens primarily serve to diminish velocity fluctuations aligned with the predominant flow direction, while exerting negligible impact on the overall flow orientation. Moreover, empirical evidence underscores that employing a series of screens characterised by varying mesh density (coarse, fine, medium), yields superior effectiveness compared to the use of a solitary finely meshed screen.

For optimal turbulence management, screens featuring a porosity falling within the range of 0.58 to 0.8 prove beneficial. However, screen porosity values exceeding 0.8 are not viable for achieving effective turbulence control, whereas the values that are lower than 0.58 result in disruptive flow instability.

$$\text{Area occupied by the screen wire} = n_w l d_w + n_w l d_w - n_w (n_w d_w^2) \tag{4}$$

$n_w$ : Mesh generic wire number
$l$ : Cross-section side of settling chamber
$d_w$ : Wire diameter

$$\text{Screen Porosity}, \beta_s = \frac{A_{flow}}{A_{total}} = \frac{l^2 - 2n_w l d_w + {n_w}^2 {d_w}^2}{l^2}$$

$$= 1 - 2n_w \frac{d_w}{l} + {n_w}^2 \frac{{d_w}^2}{l^2} = \left(1 - \frac{n_w d_w}{l}\right)^2 \tag{5}$$

Screen mesh density is characterised as the correlation between the count of mesh wires and the cross-sectional dimension of the chamber in which the screens are securely positioned.

$$\text{Mesh density}, \rho_m = \frac{n_w}{l} \tag{6}$$

Screen mesh divides($w_m$) are represented by the mesh density inverse.

$$w_m = \frac{1}{\rho_m} \tag{7}$$

$$\text{Porosity}, \beta_s = (1 - d_w \rho_m)^2 \tag{8}$$

### 2.4 Spacing Between the Screens

To ensure the complete independence of pressure drops across screens, it is imperative that the spacing is chosen in such a manner that the static pressure has fully stabilized from any disturbances before progressing to the subsequent screen installation.

For attaining the maximum advantages in terms of reducing turbulence, it is recommended that the minimum spacing aligns with the scale of the larger energy-containing eddies within the flow. Empirical observations have demonstrated that an effective combination involves employing a screen with an approximate spacing equivalent to 0.2 times the diameter of the settling chamber.

Moreover, an optimal gap between the last screen and the entry point of the contraction is also crucial, with a spacing of about 0.2 times the cross-sectional diameter yielding successful outcomes. Deviating from this guideline, if the gap is excessively short, the flow across the last screen may endure significant distortion. Conversely, if this distance is extended excessively, and the settling chamber length becomes too substantial, the undesirable consequence of excessive boundary layer formation becomes prevalent.

## 3. METHODOLOGY

The computational procedure commences with the initiation of grid generation for the settling chamber, visually depicted in Fig. 2. The grid generation process was conducted utilizing the commercial solver HYPERMESH solver. Employing an unstructured cell-based volumetric mesh approach, a meticulously refined boundary layer mesh configuration was created along the distinct sections of the settling chamber.

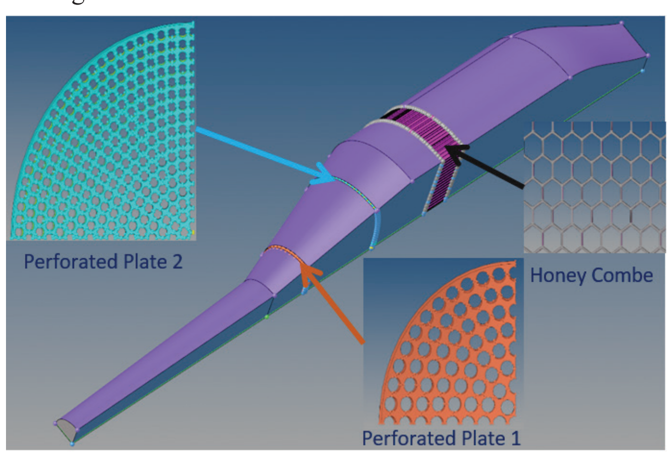


**Figure 2. Model of settling chamber.**

A mesh-independent study is carried out to ensure the result is independent. Finally, 44 million elements with a 20 prism layer grid were chosen for simulation to achieve the y+ value of less than 5. Numerical simulations concerning the settling chamber were carried out using a ANSYS Fluent solver. The simulations adopted a coupled flow solver approach, and the air within the system was modeled as an ideal gas. The density-based solver method was executed. For viscous simulations the simulation parameters were configured to encompass the viscous regime, aptly chosen for modeling turbulent flow due to the nature of the compressible subsonic flow under consideration. To accurately account for flow separation within the settling chamber, the k-ω SST turbulence model was employed[14-18].

### 3.1 Boundary Conditions

For CFD study, the settling chamber's quarter geometry was modelled using a symmetry boundary. The quarter model is used to save computational time and because wire mesh modelling in CFD is difficult. We used a mathematical approach with a porous jump instead of wire mesh. In a numerical simulation with a mass flow exit, we set a mass flow inlet boundary condition. Table 3 shows the specifics of the boundary conditions for all three cases.

**Table 3. Boundary conditions**

| | | |
|---|---|---|
| Inlet type: Mass flow inlet turbulence intensity = 20 % | Case 1 | $\dot{m}$ = 75 kg/s |
| | | Static pressure, $P_s$ = 3.35 bar |
| | Case 2 | $\dot{m}$ = 300 kg/s |
| | | Static Pressure, $P_s$ = 8.98 bar |
| | Case 3 | $\dot{m}$ = 87 kg/s |
| | | Static Pressure, $P_s$ = 22.6 bar |
| Outlet type: mass flow outlet | Case 1 | $\dot{m}$ = 75 kg/s |
| | Case 2 | $\dot{m}$ = 300 kg/s |
| | Case 3 | $\dot{m}$ = 87 kg/s |
| Wall | | No slip |
| Symmetry | | Symmetry |

## 4. RESULTS AND DISCUSSION

From the performance analyses of the setting chamber, the results indicate that the total pressure is constantly decreasing in the connecting pipe section, which has a low divergent section, and there is a sudden decrease of total pressure observed in the diffuser section, which indicates the loss in that section is large. To minimize the flow separation loss, the perforated plates are kept at the optimal distance. As illustrated in Fig. 3, there is a minimum loss as the flow passes through the honeycomb in the constant area portion, where the loss is only caused by frictional effects.

An increase in static pressure is noted in the connecting pipe due to an increase in the area caused by the diverging portion. Because of the accelerated flow through the perforations, the static pressure decreases after the perforated plates. As illustrated in Fig 4, the static pressure tends to drop during the contraction portion due to the decrease in area.

The flow is almost stable after the honeycomb, as shown in Fig. 5. There is some flow recirculation after the perforated plates, and the flow velocity in the constant diameter portion is

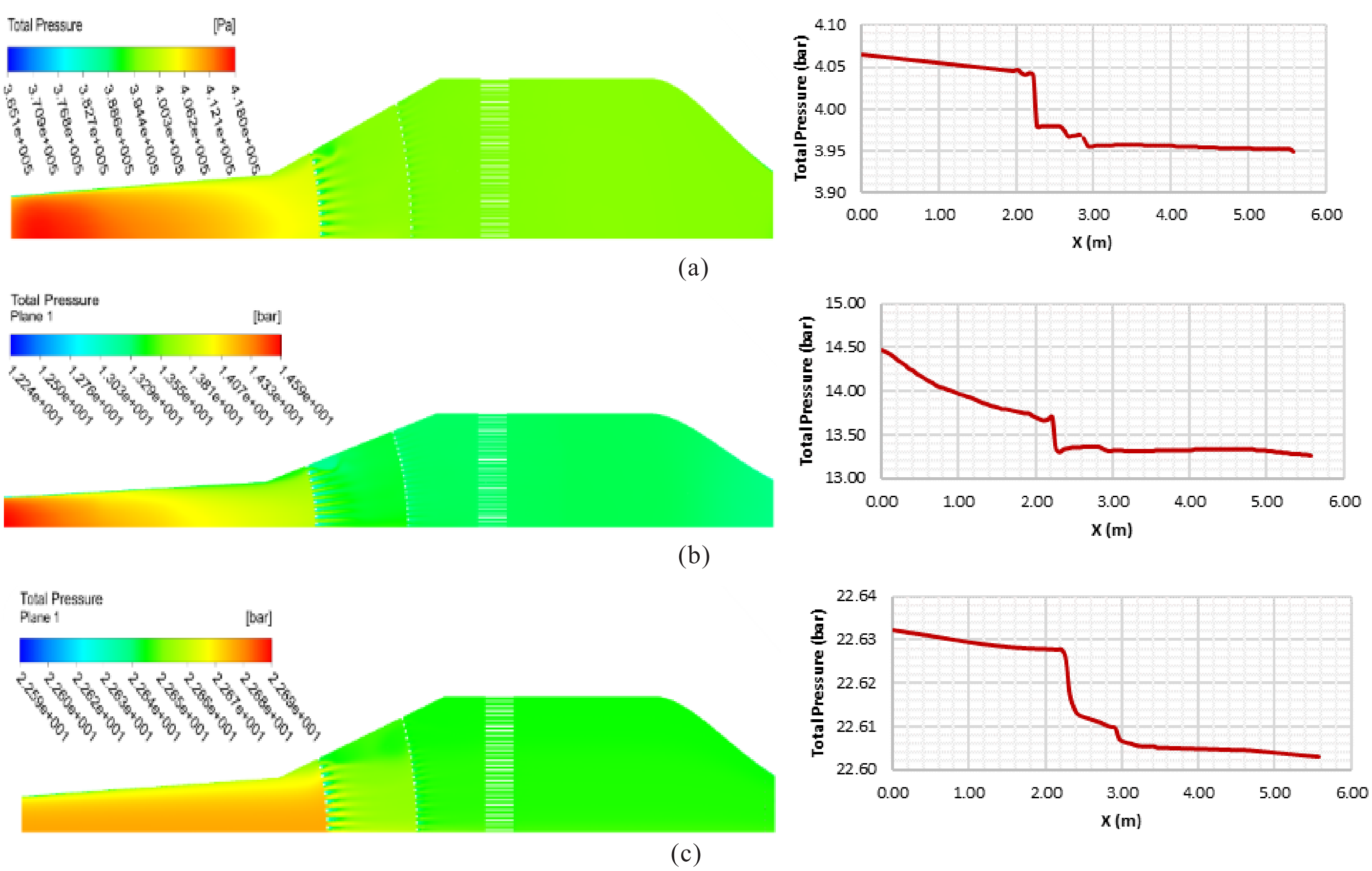


**Figure 3. Total pressure in XY plane and average total pressure along X-axis, (a) Case-1; (b) Case-2; and (c) Case-3.**

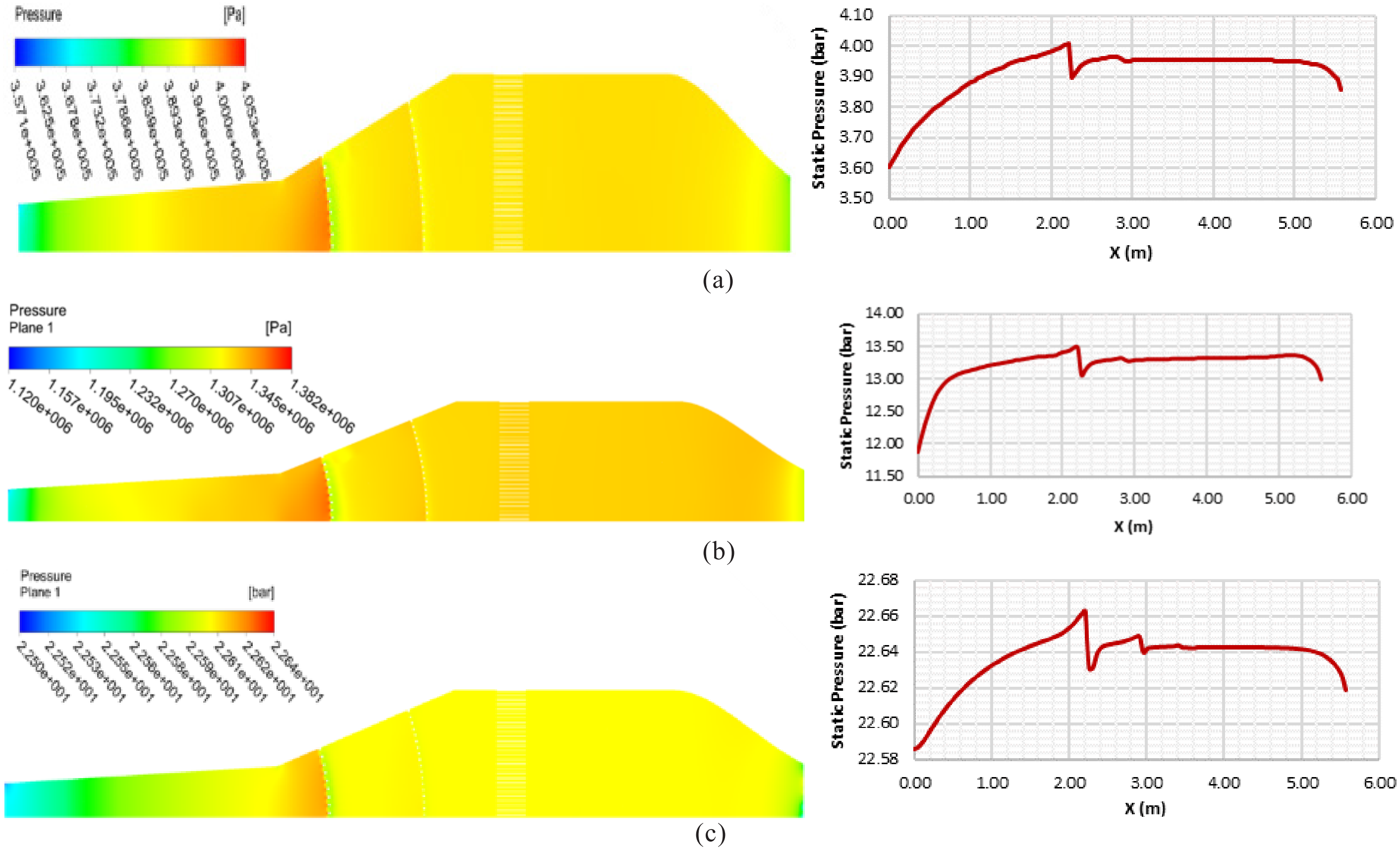


**Figure 4. Static pressure in XY plane and average static pressure along X-axis, (a) Case-1; (b) Case-2; and (c) Case-3.**

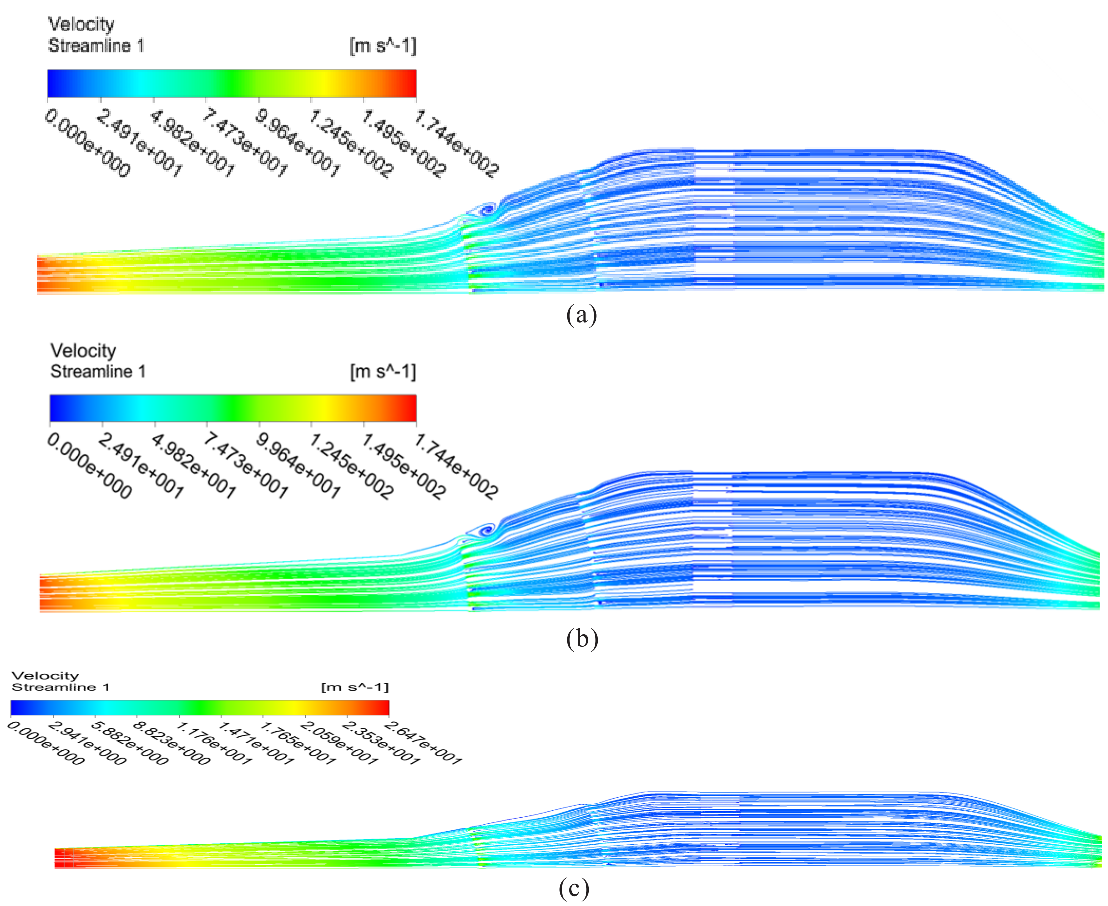


**Figure 5. Velocity streamline in XY plane, (a) Case-1; (b) Case-2; and (c) Case-3.**

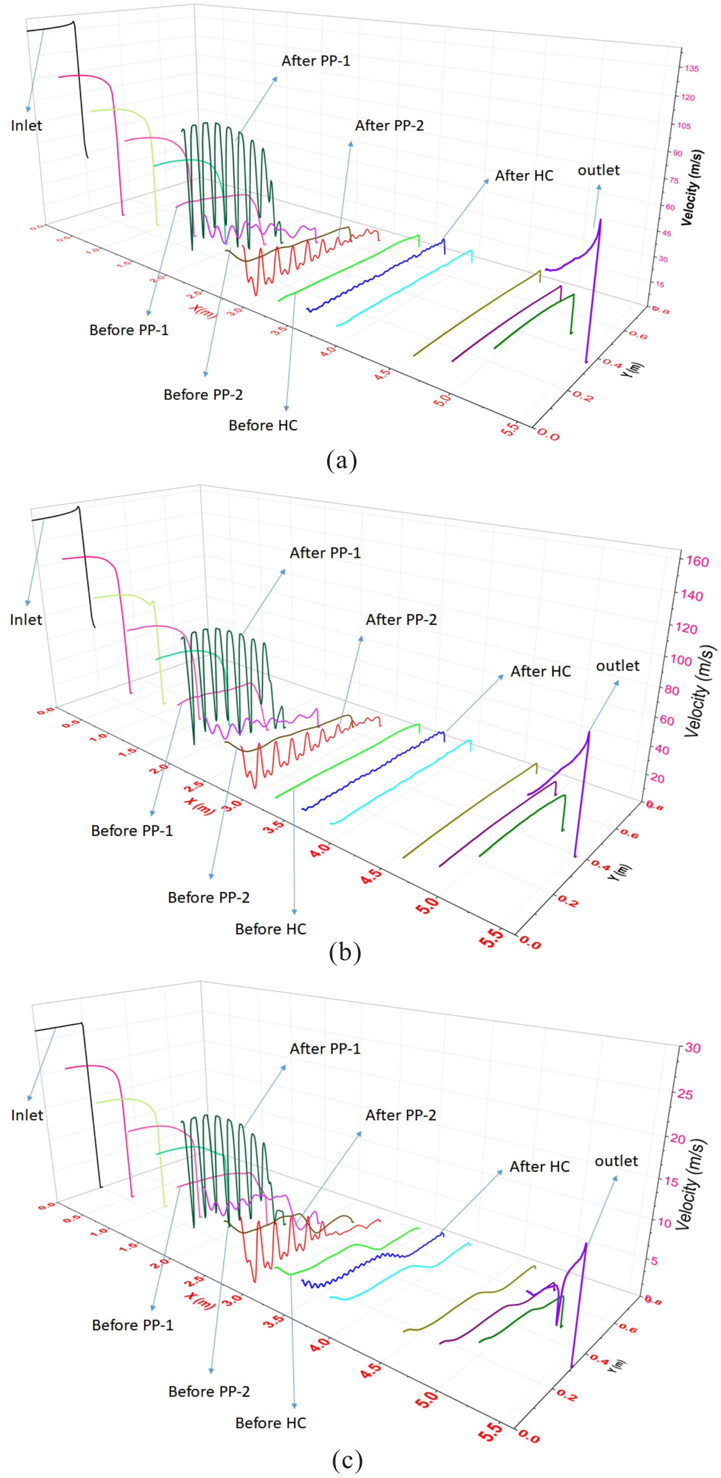


Figure 6. Radial velocity 3D plot, (a) Case-1; (b) Case-2; and (c) Case-3.

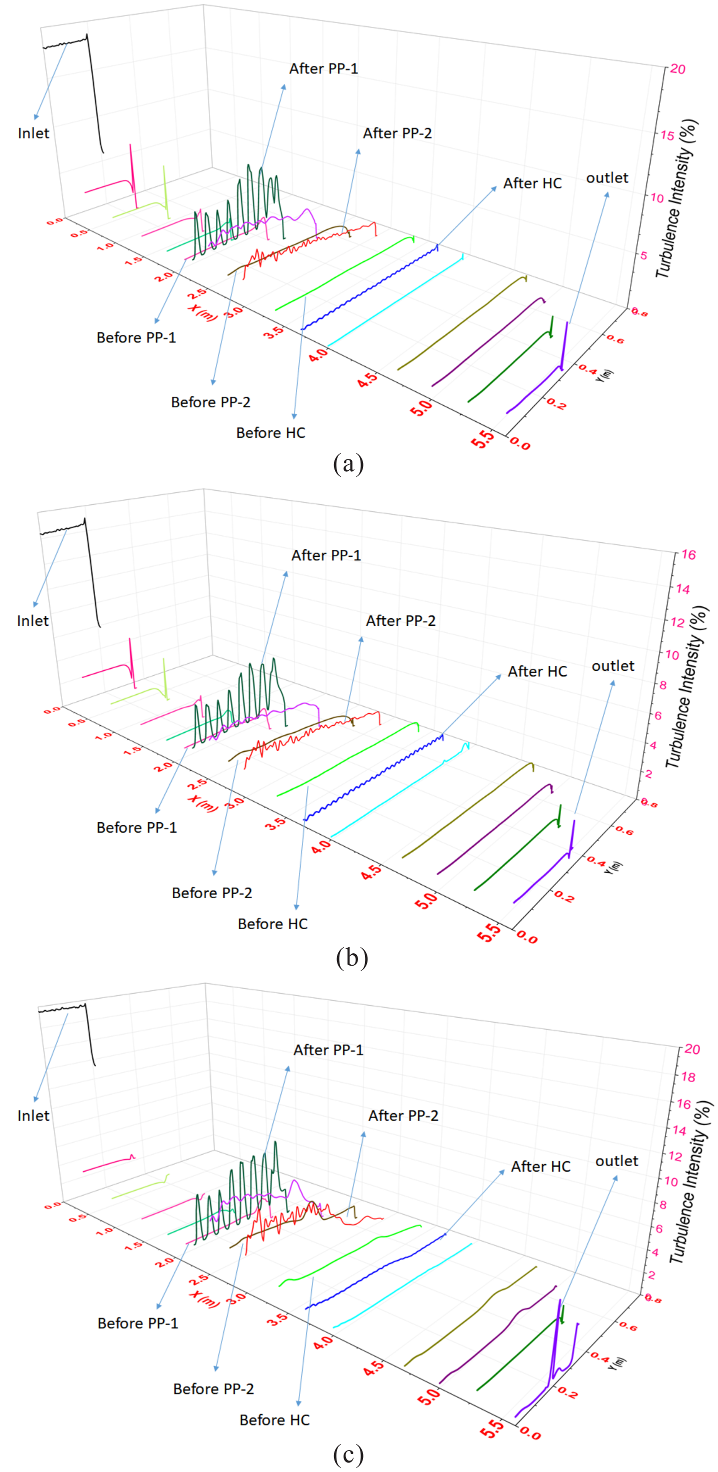


Figure 7. Radial turbulence intensity 3D plot, (a) Case-1; (b) Case-2; and (c) Case-3.

30 m/sec, which is consistent with the design requirement. The radial velocity variation is illustrated in Fig. 6.

The intensity of turbulence is proportional to the hydraulic diameter. Even though the inlet turbulence is 20 %, it quickly dissipates to the pipe's maximum handling capacity and then steadily declines. There is a sudden increase in turbulence after the perforated plates due to the creation of the vortices while the flow passes through the perforations. Local turbulence at the outlet causes a sudden increase in turbulence strength as it exits the settling chamber. Figure 7 shows, in all three cases, the overall turbulence intensity was reduced from 20 % to less than 1 %. This demonstrates that the flow pressure fluctuations have been minimized to an acceptable level.

### 4.1 Theoretical Calculation of Turbulence Reduction by Screens

Incorporating an accurate representation of the wire mesh within the settling chamber within the model presents substantial computational demands, primarily attributed to the delicate and slender cross-sectional profile of the wire mesh. As detailed by Laws, E.M.[19], *et al.* theoretical calculations offer a predictive approach to anticipate the reduction in turbulence resulting from the strategic positioning of the screens.

Theoretical Calculation of wire mesh with Turbulence Reduction Factor Mesh/inch: 10, Wire diameter: 0.009 inches (0.2286 mm), Porosity: 0.46 is as follows.

$$K = \frac{2 \times \Delta P}{\rho \times V} \tag{9}$$

$$Re = \frac{V \times d}{\text{kinematic viscosity}} = 532.5\ m \tag{10}$$

$$\text{For } 40 < Re < 105 \tag{11}$$

$$K = \left(0.52 + \left(\frac{66}{Re\left(\frac{4}{3}\right)}\right)\right)\left(\frac{(1-\beta_2)}{\beta_2}\right) = 0.57 \tag{12}$$

Turbulence Reduction Factor:

$$F_u = \frac{1}{\sqrt{(1+K)}} = 0.79 \tag{13}$$

The flow turbulence after passing through wire mesh 1 is 0.00165. Furthermore, the turbulence reduction factor for wire mesh 2 and 3 was determined. The flow turbulence after passing through wire mesh 2 is 0.0012, and it is 0.000941 after passing through wire mesh 3.

## 5. CONCLUSION

Computational Fluid Dynamics (CFD) investigation was conducted on the settling chamber within the Tri-Sonic Wind Tunnel, encompassing three distinct scenarios involving varying mass flow rates and pressure conditions. The analyses showed flow recirculation before and after the first Perforated Plate(PP-1) for each of the three mass-flow rate settings. However, after the flow goes through the second Perforated Plate (PP-2), this recirculation is eliminated.

Losses resulting from flow separation are also minimised due to a decrease in flow recirculation. Therefore, it can be said that perforated plates do significantly reduce pressure loss. The analyses in the constant area section show that the honeycombs do avoid flow recirculation, which minimises turbulence.

After introducing the honeycomb, it is discovered that the flow is uniform. Local turbulence can also be noticed at the settling chamber's outlet. It can be interpreted as the result of using mass-flow rates to define the input and output conditions in Fluent.

Defining the inlet and outlet conditions using mass-flow rates makes it highly unstable since the total pressure is left undefined. Additionally, it makes achieving convergence challenging. Because this local turbulence is thought to be the result of a software-specific computational error, we have opted to disregard it.

The pressure loss and turbulence reduction caused by the wire meshes in these CFD simulations are not assessed. Then, it was simulated using traditional analytical and empirical methods found in recent studies. The simulated turbulence at the outflow was discovered to have been further diminished, and the flow is anticipated to be more uniform than what was predicted using CFD alone.

Initially, a simulation of the impact of wire mesh on the flow was performed using theoretical calculations and the assumption that the mesh was porous. Finally, in all three cases, the flow downstream of the honeycomb is uniform, and the average turbulence intensity level is lowered to 1 % compared to the inlet turbulence intensity level of 20 %.

## REFERENCES


1. Özahi, E. An analysis on the pressure loss through perforated plates at moderate reynolds numbers in turbulent flow regime. *Flow Meas. Instrum.*, 2015, **43**, 6–13. doi:10.1016/j.flowmeasinst.2015.03.002
2. Zhao, T.; Zhang, J. & Ma, L. A general structural design methodology for multi-hole orifices and its experimental application. *J. Mech. Sci. Technol.*, 2011, **25**(9), 2237-2246. doi: 10.1007/s12206-011-0706-3
3. Mehta, R.D. The aerodynamic design of blower tunnels with wide angle diffusers. *Prog. Aerosp. Sci.*, 1977, **18**, 59-120. doi: 10.1016/0376-0421(77)90003-3
4. Mehta, R.D. & Bradshaw, P. Design rules for small low-speed wind tunnels. *Aeronaut. J.*, 1979, **83**(827), 443–453. doi: 10.1017/S0001924000031985
5. Bradshaw, P. & Pankhurst, R.C. The design of low-speed wind tunnels. *Prog. Aerosp. Sci.,* 1964, **5**, 1–69. doi: 10.1016/0376-0421(64)90003-X
6. Okolo, P.N.; Zhao, K.; Kennedy, J. & Bennett, G.J. Numerical modelling of wire screens for flow and noise control. *In* AIAA/CEAS Aeroacoustics Conference, 2017. doi: 10.2514/6.2017-3700
7. Dryden, L. The use of damping screens for the reduction of wind-tunnel turbulence. *J. Aeronaut. Sci.*, 1947,**14**(4), 221–228. doi: 10.2514/8.1324
8. Schubauer, G.B.; Spangenberg, W.G. & Klebanoff, P.S. Aerodynamic characteristics of damping screens. NASA Technical Reports Server, 1950.
9. Guo, B.Y.; Hou, Q.F.; Yu, A.B.; Li, L.F. & Guo, J. Numerical modelling of the gas flow through perforated plates. *Chem. Eng. Res. Des.*, 2013, **91**(3), 403-408. doi: 10.1016/j.cherd.2012.10.004
10. Roach, P. The generation of nearly isotropic turbulence by means of grids. *Int. J. Heat Fluid Flow*, 1987, **8**(2), 82-92. doi: 10.1016/0142-727X(87)90001-4
11. Scheiman, J. & Brooks, J.D. Comparison of experimental and theoretical turbulence reduction from screens, honeycomb, and honeycomb-screen combinations. *J. Aircraft*, 1981,**18**(8), 638-643.
12. Sachin, B. Pressure losses in an isolated perforated plate and jets emerging from the perforated plate. *Int. J. Mech. Sci.*, 1989, **31**(1), 51-61. doi: 10.1016/0020-7403(89)90118-5
13. Sachin, B. & Ward-Smith, A.J. The use of perforated plates to control the flow emerging from a wide-angle diffuser, with application to electrostatic precipitator

design. *Int. J. Heat Fluid Flow*, 1987, **8**(2), 124–131.
doi: 10.1016/0142-727X(87)90011-7
14. Chakraborty, D. Forty years of computational fluid dynamics research in India-achievements and issues. *Defence Sci. J.*, 2010,**60**(6), 567-576.
doi: 10.14429/dsj.60.601
15. Dharavath, M. & Chakraborty, D. Numerical simulation of supersonic jet impingement on inclined plate. *Defence Sci. J.*, 2013, **63**(4), 355-362.
doi: 10.14429/dsj.63.2545
16. Premkumar, P.S.; Pillai, S.N. & Senthilkumar, C. Study on oil-cooler location for a pusher type turbo prop aircraft using numerical simulation. *Aircraft Eng. Aerosp. Technol.*, 2022, **94**(6), 895-905.
doi: 10.1108/AEAT-08-2021-0228
17. Saha, S. & Chakraborty, D. Hypersonic intake starting characteristics–A CFD validation study. *Defence Sci. J.*, 2012, **62**(3), 147-152.
doi: 10.14429/dsj.62.1340
18. Murty, M.; Chakraborty, D. & Mishal, R. Numerical simulation of supersonic combustion with parallel injection of hydrogen fuel. *Defence Sci. J.*, 2010, **60**(5), 465-475.
doi: 10.14429/dsj.60.57
19. Laws, EM.& Livesey, JL. Flow through screens. *Annu. Rev. Fluid Mech.,* 1978, **10** (1), 247–266.
doi: 10.1146/annurev.fl.10.010178.001335

## CONTRIBUTORS

**Mr K. Balaji** holds the position of Project Engineer at the Kumarguru Center for Industrial Research and Innovation, situated within Kumaraguru College of Technology. His areas of research include: Computer-aided drafting and hypermesh applications.
In the current study, he conducted simulations and experimental studies, and then composed the initial manuscript.

**Mr H. Sathish** is a Project Engineer of Kumarguru Center for Industrial Research and Innovation, Kumaraguru College of Technology. His areas of research include: Fluent analysis. In the current study, he executed the experiment, formulated the problem statement, conducted simulations and experimental studies, and authored the preliminary manuscript.

**Mr G. Balu** is a Scientist and Technology Director at the DRDO-Directorate of Aerodynamics, DRDL, Hyderabad. In the current study he provided guidance during the manuscript review process, offering valuable input on formulation and results.

**Prof. V. Shanmugam** is a Distinguished Scientist affiliated with DRDO-Directorate of Aerodynamics, DRDL, Hyderabad. In the current study, he guided during the manuscript review and contributed valuable insights to the formulation and results.

**Prof. Prakash Singh** is a Distinguished Scientist affiliated with the DRDO-Directorate of Aerodynamics, DRDL, Hyderabad.
In the current study, he directed in the manuscript review process and offered valuable insights into the formulation and results.

**Dr V. Gautham** is working as a Research Faculty at the Kumaraguru Center for Industrial Research and Innovation, Kumaraguru College of Technology. His areas of research include: Investigations into the structural integrity of nuclear reactor roof slabs, static and fatigue analyses of automotive side-step assemblies, design studies for lightweight aluminum structures in maritime environments, evaluations of pipe clamp assemblies, finite element analyses of cone crushers, and numerical investigations concerning ESM RF LRU applications on aircraft.
In the current study, he undertook the responsibility of arranging and organising the manuscript, ultimately playing a role in the final composition.

**Prof. C. Vasantharaj** is the Director of Kumaraguru Center for Industrial Research and Innovation Kumaraguru College of Technology. His areas of research include: Supersonic wind tunnel design & calibration at DRDL, design of hypersonic wind tunnel, wind tunnel testing of Akash Intake, Prithvi Nose Cone opening, design and fabrication of Pinaka rockets, wind tunnel model design & testing of Rustom UAV, CFD simulation for sabot separation for 125 mm FSAPDS ammunition, penetration performance of projectile impacting on targets comprising of concrete and soil.
In the current study, he guided through the manuscript review process, offering valuable perspectives on formulation and results.

**Prof. P.S. Prem Kumar** is an Associate Professor of the Aeronautical Engineering Department Kumaraguru College of Technology.
In the current study, he conceptualised the problem statement, conducted a manuscript review, and contributed valuable insights to the formulation and results.